

Temperature Distribution of Radiofrequency Hyperthermia in a Capacitance System in Breast Equivalent Tumor Ablation: A Simulation Study

Seyed Erfan Saadatmand¹, Seyede Mahsa Kavousi¹, Nader Riahi Alam^{1,2*}

1. Department of Medical Physics and Medical Engineering, Faculty of Medicine, Tehran University of Medical Sciences, Tehran, Iran.
2. Concordia University, PERFORM Center, Montreal, Quebec, Canada.

ARTICLE INFO

Article type:
Original Paper

Article history:

Received: Jun 08, 2019
Accepted: Dec 27, 2019

Keywords:

Computer Simulation
Finite Element Analysis
Breast Cancer
Radiofrequency Ablation
Hyperthermia

ABSTRACT

Introduction: For decades, hyperthermia had been widely used for tumor ablation by increasing the temperature of cancerous tissues. For clinical treatment, a capacitance system was developed around the world. In this study, a capacitance system of radiofrequency (RF) hyperthermia was simulated to achieve the temperature distribution map of the entire breast equivalent phantom. Therefore, the efficiency of this method in the treatment of breast cancer was investigated in the current study.

Material and Methods: In this study, an RF system with a frequency of 13.56 MHz was simulated by Comsol Multiphysics software (Version 5.3). The geometry of the breast cancerous tissue was modeled by the consideration of three different tissues, including the fat, gland, and tumor tissues. The two electrodes of the system were modeled as two disks with a radius of 15 cm. The calculations of the RF wave and bioheat equation were accomplished by numerical simulation and finite element method.

Results: The temperature plots were obtained in 5 min. The temperature distribution map was entirely achieved and the results were compared with experimental findings to check the accuracy of the RF device and precision of the thermometer.

Conclusion: The obtained results showed that the temperature of the whole tumor region increased uniformly (3-4°C). Moreover, the temperature of the whole healthy tissues (i.e., the gland and fat tissues) did not increase (1.9-2.1°C). Consequently, in the capacitive hyperthermia system, the tumor reached extreme heat; however, the healthy tissues were completely protected from damages.

► Please cite this article as:

Saadatmand SE, Kavousi SM, Riahi Alam N. Temperature Distribution of Radiofrequency Hyperthermia in a Capacitance System in Breast Equivalent Tumor Ablation: A Simulation Study. Iran J Med Phys 2021; 18: 40-48. 10.22038/ijmp.2019.40969.1583.

Introduction

The lethal disease and mortality cause in women worldwide is breast cancer [1]. Despite progressive achievements in clinical treatment, the treatment process of the most breast cancer patients still continues to fail. The mortality rate of the disease has been reported to be on the rise typically due to the metastasis [2-4]. Hyperthermia is an adjuvant approach for cancer treatment which increases body temperature. According to the comparatively high thermal sensitivity of tumor cells, compared to that reported for healthy cells, hyperthermia has been studied for decades [5, 6].

The temperature rise can occur by various techniques, such as radiofrequency (RF), microwave hyperthermia, magnetic hyperthermia, perfusion therapy or laser ablation [7, 8]. Hyperthermia is mostly identified within a range of temperatures from 40 to 48°C or similarly maintains the temperature at the desired site for about an hour or more [9-12]. This amount of increase in temperature can cause damage in tumor cells; nevertheless, normal tissues can tolerate it. In the beginning, capacitive hyperthermia

devices were basically used in Asian countries. In comparison to the radiative systems, this system is more affordable and easy-to-use. Therefore, nowadays, the application of this system developed in the Western world [13, 14].

In hyperthermia, two different kinds of properties are important and should be examined, namely dielectric and thermal characteristics. Most of the studies have not simultaneously considered both properties of this method [2, 13, 14] or have failed to use proper geometry in the development of breast phantoms [3, 4]. In addition, some of these studies have not investigated the glandular tissues of the breast [15]. In some studies, all these issues were considered; however, the phantom was not utilized for experimental studies [16].

According to the evidence [17], the frequency is inversely proportional to the depth of penetration. In 900 MHz, 4.2 cm depth of body can be reached, and frequencies above this amount cannot be used for breast tumors in clinical treatments. In a previous study, a suitable geometry for breast was designed,

*Corresponding Author: Tel: +98 09121909646; E-mail: RiahiAlam@gmail.com

and a phantom with an oil-gelatin mixture with similar thermal and dielectric properties to a real breast was fabricated. After measuring the properties of the phantom, this phantom was put in an electromagnetic field with a frequency of 13.56 MHz. Eventually, the thermal effects on breast equivalent phantom were examined within the frequency range of 10-15 MHz, which is widely used in clinical treatments [18].

The experimental and simulation results were compared in the current study. All the experimental conditions including the clinical device, as well as the geometry and properties of the phantom, were investigated in Comsol multiphysics software (developed in COMSOL Inc. company, Sweden). The present study aimed to achieve the temperature distribution map of the breast equivalent phantom, validate the experimental study, and compare their results. Moreover, the accuracy of the RF device and precision of the thermometer are checked. The bioheat transfer equation was calculated by Comsol multiphysics software, and the temperature plots were obtained at each point of the phantom. The frequency used in this study was 13.56 MHz similar to that reported in a previous study on clinical treatments. The frequencies within the range of 10-15 MHz are suitable in clinical therapies. In this band, the penetration depth is well enough to cover the whole body, and this band can cause ablation in tumor cells with the least damage to healthy tissues.

Materials and Methods

Experimental

This section is divided into five parts, including designing geometry, fabricating phantom, measuring thermal and dielectric properties, disposing phantom in RF radiation, and calculating a specific absorption rate (SAR). Each part is explained in detail in the following subsections:

Geometry design

In this part, a proper geometry in SolidWorks software (version 2018) was designed, which represented the real breast. Three different tissues of a cancerous breast were considered, including fat, gland, and tumor tissues. A 5 cm radius hemisphere was designed as a whole breast, with a 3.5×5 cm diameter semi-oval embedded in it. This semi-oval represented the gland tissue, and the distance between the hemisphere and semi-oval showed the fat tissue. At the bottom of this semi-oval, there was a sphere with a radius of 1 cm as a tumor region. As shown in Figure 1, this geometry is utilized with a 3D printer (Sizan Company, Iran).

Fabrication of phantom

The properties of the oil-gelatin phantom are similar to real tissues [10]. For instance, agar mixtures have a high melting point (approximately 80°C); therefore, they can preserve their shape. However, their permittivity is

lower than the real tissues. Consequently, they cannot represent the dielectric properties of tissues [14]. TX-150 can successfully provide for tissues with high water amount, such as the tumor tissues; however, it cannot be used for tissues with low water amount, such as the fat tissues [10]. Nevertheless, the oil-gelatin mixture can be easily prepared homogeneously, and by the addition of formaldehyde, their shape maintains at high temperatures. Therefore, their behavior in an electromagnetic field in hyperthermia represents real tissues much more than other materials.

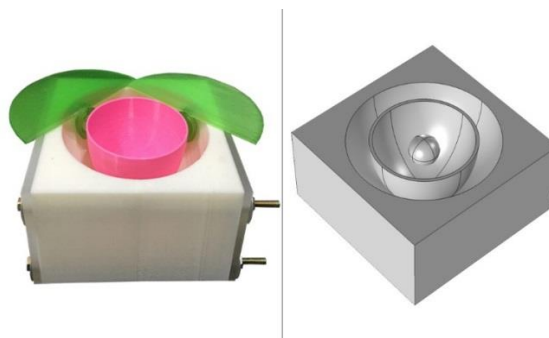


Figure 1. The design of phantom and the 3D-printed of the phantom



Figure 2. Cube for fabrication of tumor tissue with a hole in it for injection of mixture



Figure 3. Oil-gelatin phantom of breast

In the present study, the main materials for fabricating phantom were calfskin gelatin (sigma), safflower oil, and water. Adding NaCl to the mixture helped to adjust electrical conductivity (σ) for tumor tissue. The amount of the specific heat capacity of oil is minor than water (specific heat capacity of oil is about 1.64 [J/kg°C]; however, it is 4.42 [J/kg°C] for water). Consequently, for adjusting these properties in tissues with high specific heat capacities, such as tumor and gland tissues, water was used instead of oil.

Table 1. Weight of each material in each tissue

Material \ Tissue	Oil (g)	Gelatin (g)	Water (g)	Salt (g)	Surfactant (g)	Formaldehyde (g)
Fat	121.49	13.69	35.93	0	6.8	2.16
Gland	24.68	32.81	98.74	0	1.38	1.73
Tumor	1	1.9	5.7	0.18	0.07	0.11

Table 2. Values of thermal properties in each tissue of phantom with real values of breast tissues

Tissue		Fat	Gland	Tumor
Specific heat capacity (J/kg ²)	Real amount	2,280	3,639	3,639
	Measured amount	2,300	3,670.5	3,670.5
Thermal conductivity (W/m ²)	Real amount	0.3	0.56	0.56
	Measured amount	0.3	0.56	0.56
Density (Kg/m ³)	Real amount	1,069	1,050	1,050
	Measured amount	1,070	1,048	1,048

The prepared mixture in the current study contained both hydrophilic and hydrophobic materials. Therefore, sodium lauryl sulfate was used as a surfactant in order to bring homogeneity to the phantom. In order to stabilize the phantom at high temperatures, formaldehyde was added to the mixture to increase its melting point and prevent its transfiguration [8]. The weight values of materials for each tissue are shown in Table 1.

For the fabrication of this phantom, the fat mixture was initially made and filled in a region of the phantom prepared as a fat layer. According to Lazebnik et al., the researchers waited at least 5 days since formaldehyde cross-linking of gelatin to be completed [8]. Then, the gland mixture was created, and after 5 days, the phantom was divided into two parts for putting a tumor. For making the tumor sphere with a radius of 1 cm, a cube was used, which had a spherical hole with a radius of 1 cm in it (Figure 2). The final phantom is depicted in Figure 3.

Measurement of thermal and dielectric properties

After fabricating the phantom, the thermal and the dielectric properties of the phantom were measured and compared with real breast tissues. For the measurement of thermal properties (i.e., specific heat capacity, thermal conductivity, and density), nine samples were taken from different parts of each tissue to improve measurement accuracy, and their amount was measured by a calorimeter (IKA company, Germany). The thermal properties are shown in Table 2.

Generally, the dielectric properties include relative permittivity and conductivity. The permittivity is described as a complex physical quantity that contains a real part and an imaginary part. The real part is defined as the ability of a medium to store electric field energy, and the imaginary part is defined as a loss factor that describes the dissipated energy in the material [10]. The complex permittivity is expressed as follows:

$$\varepsilon = \varepsilon' - j\varepsilon'' \quad (1)$$

where ε , ε' and ε'' are the complex permittivity (F/m), real part of the permittivity, and imaginary part of the permittivity (i.e., loss factor), respectively. The permittivity calculations in the complex form had multiple difficulties; therefore, some simplifications and capacitor concepts were used in this regard. According to the capacity equation of capacitor, the capacity of a capacitor in the air to medium describes the complex permittivity. Also, normalizing the permittivity of tissues to vacuum represents relative permittivity. Equations 2 and 3 denote the relative permittivity and conductivity relations as follows:

$$\varepsilon_r = \frac{C}{K} \quad (2)$$

$$\sigma = \frac{G\varepsilon_0}{K} \quad (3)$$

where C , K , ε_0 , and G are the capacitance of the capacitor in tissue (F), capacitance of the capacitor in the air (F), permittivity of free space (F/m), and conductivity of the capacitor (S/m), respectively. Table 3 tabulates the dielectric properties of the phantom.

Behavior of phantom in radiofrequency radiation

After the measurement of properties, the phantom was placed in an RF field using a Celsius TCS device (Celsius 42+ GmbH, Cologne, Germany) with a frequency of 13.56 MHz (Figure 4a). The device is composed of two pairs of electrodes in two sizes of 15 and 25 cm (Figure 4b), which are located on the top and below of the phantom.

Table 3. Values of dielectric properties in each tissue of phantom

Tissue	Fat	Gland	Tumor
Relative permittivity ϵ_r	11.8	138.4	142.5
Electrical conductivity $\sigma(S.m^{-1})$	0.03	0.63	0.71

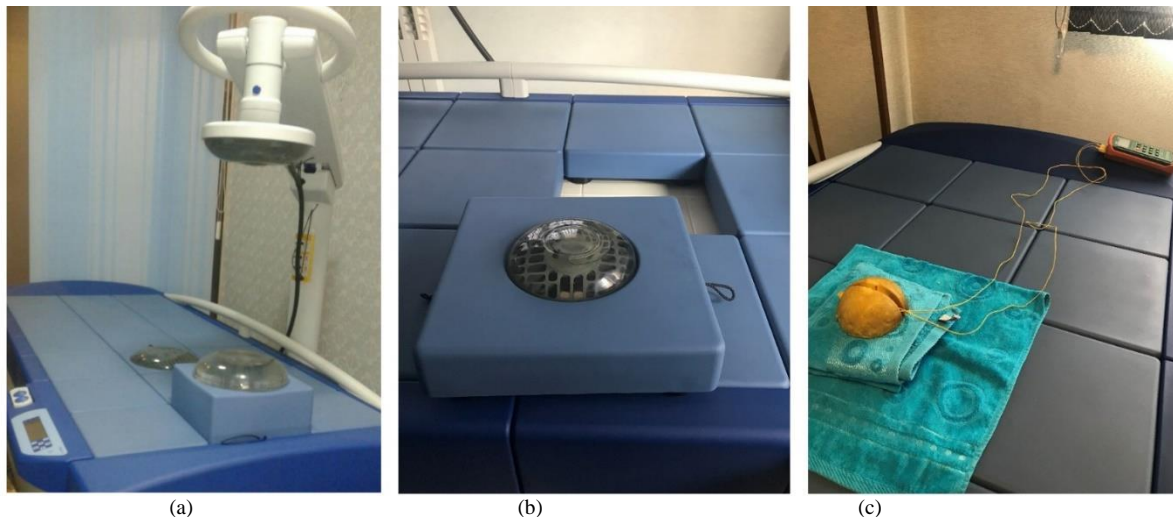


Figure 4. (a) Celsius TCS (Celsius42+ GmbH, Cologne, Germany); (b) bottom electrode (150 mm) of device; (c) phantom on hyperthermia device; shifting up the phantom for adjustment of tumor on focus point

Simulation Modeling

The geometry of the breast, including the fat, gland, and tumor tissues, was modeled in three dimensions in Comsol multiphysics software. Figure 5 depicts the modeled geometry with the sizes of different tissues. The two electrodes in the form of the two circular disks with a radius of 15 cm were modeled along the z-axis. The cold water bolus was simulated similar to clinical devices. When the same size electrode was used at each side, focusing occurred in the central point and a maximum intensity was obtained at this point. Therefore, the simulated tumor was positioned at this point to prevent healthy tissue from extra heating. Consequently, the upper and lower bolus thicknesses were considered 5 and 9 cm, respectively. The physical parameters, including specific heat capacity, thermal conductivity, density, relative permittivity, and electrical conductivity, were applied to the model according to tables 2 and 3.

The selected amounts for simulation were chosen similar to the measured amounts in the experimental study. The calculation of RF waves used for hyperthermia was simulated by the electromagnetic module in the frequency domain condition at a frequency of 13.56 MHz. The scheme of the geometry location in the device is illustrated in Figure 6. The bioheat transfer was calculated using the Pennes' equation with the bioheat transfer module and finite element method in 5 min. The different levels of mesh refinement were tested; coarse, normal and fine meshes

(default meshes of COMSOL multiphysics software). In this model, the fine mesh was used, and the calculations were performed with 91,499 elements and 603,083 degrees of freedom.

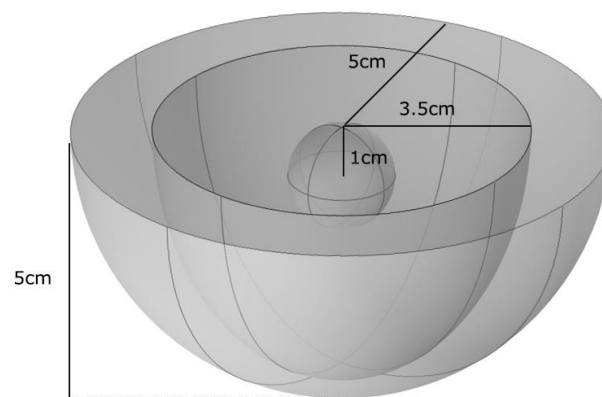


Figure 5. Modeled geometry in Comsol Multiphysics software with sizes of different tissues

Calculations of specific absorption rate

During the application of an external force, the tissues absorb the energy generated from the field. The rate of the absorbed energy by tissues is defined as SAR. In this study, the SAR is the amount of heat generated by the electromagnetic waves measured in W/m^3 [19]. By solving Maxwell's equations using the finite-difference time-domain method, the electromagnetic field was calculated for radiative heating [20]. The SAR and power density (PD) was calculated as follows:

$$PD = \frac{\sigma}{2} \|\vec{E}\|^2 = \rho SAR \tag{4}$$

where σ , \vec{E} , and ρ are the electric conductivity (S/m), electromagnetic field (V/m), and tissue density (Kg/m³), respectively.

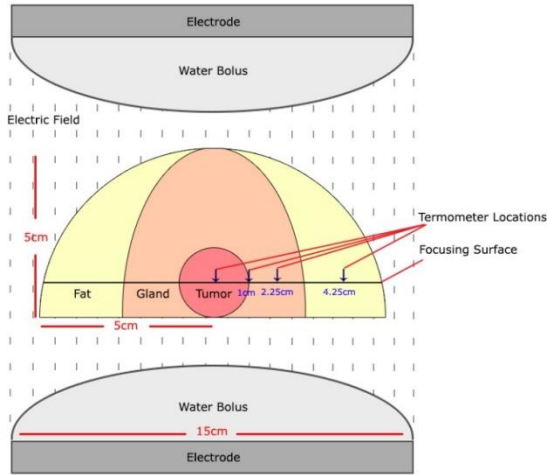


Figure 6. Scheme of geometry location in device; location of two 15 cm electrodes on the top and at the bottom; illustration of four different points of phantom for measurement

Calculations of temperature

The temperature of each point of the phantom was measured using the Pennes' bioheat equation as follows [21]:

$$c \rho \frac{\partial T}{\partial t} = \nabla \cdot (k_{tis} \nabla T) - c_b W_b (T - T_{art}) + PD \tag{5}$$

where c , k_{tis} , c_b , W_b , and T_{art} are the specific heat capacity of the tissue (J/kg°C), thermal conductivity of the tissue (W/K.m), specific heat capacity of the blood (J/kg°C), blood perfusion rate (ml/s), and local arterial or body core temperature (°C), respectively. The fabricated

breast phantom in a previous study [18] did not include the vessels and blood. Consequently, the blood perfusion rate was neglected in simulation. Therefore, the second part of the equation was considered 0 to have the same situation in experimental and simulation studies.

Results

When the same size electrodes were used at each side, focusing occurred in the central point and a maximum intensity achieved at this site. Therefore, the tumor was adjusted to this point for the prevention of healthy tissues from extra heating, particularly fat (due to low specific heat capacity). Figure 4c shows the phantom between the two electrodes. Measuring the temperature of some specific points of the phantom was achieved by a thermocouple (Extech 421509 [Extech company, U.S]) in the experimental study. Several powers and times were tested with both sizes of electrodes to identify proper parameters. After multiple tests, it was recognized that the proper power and time for the breast in this frequency was 40 W and 5 min, respectively. According to the literature [18], the temperature of the tumor center to its border was about 3-3.6°C; however, this amount for the gland and fat tissues were 1.8 and 1.6°C, respectively.

In the simulation study, all the situations of the experimental study, including the properties of the electrodes, water bolus, and distance between the electrodes, were modeled. The physical parameters of the system, including frequency, power, and time, were chosen as 13.56 MHz, 40 W, and 5 min, respectively. In the experimental study, the temperature of the four points of the phantom was measured. Nevertheless, the temperature of the entire phantom was obtained in the simulation study. The temperature distribution plots of different slice and temperature of the phantom surface are shown in figures 7 and 8, respectively.

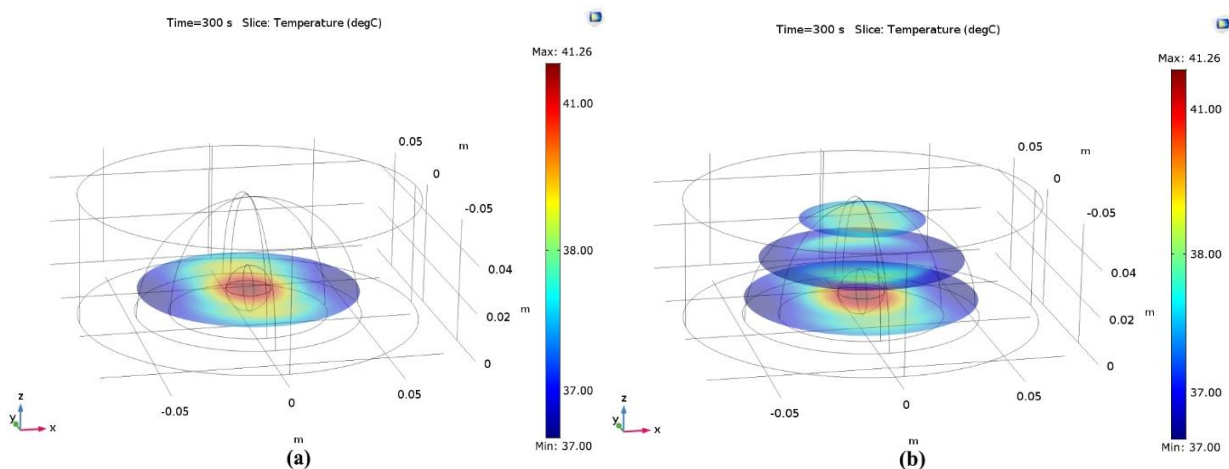


Figure 7. Different temperature distribution plots obtained from simulation in Comsol multiphysics software; (a) slice of temperature amounts from center of tumor; (b) different slice of temperature

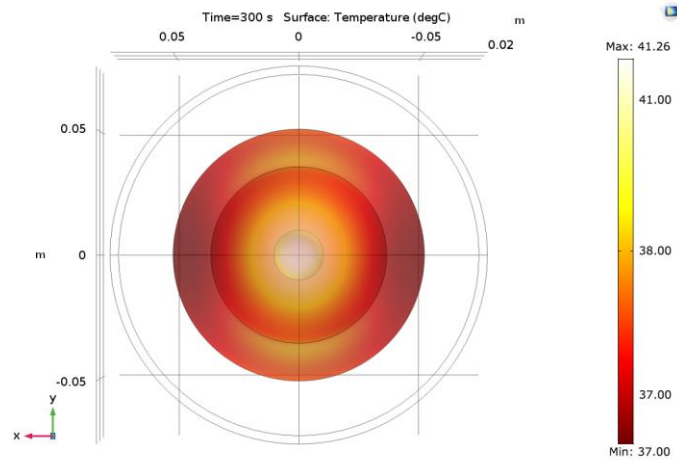


Figure 8. Temperature distribution of surface obtained from simulation in Comsol multiphysics software

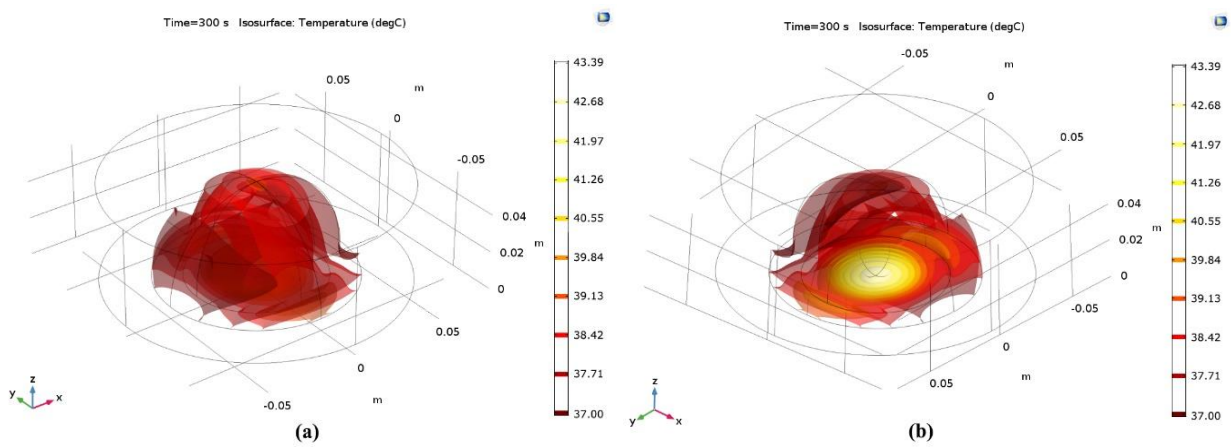


Figure 9. Isosurface temperature distribution plots in two different views

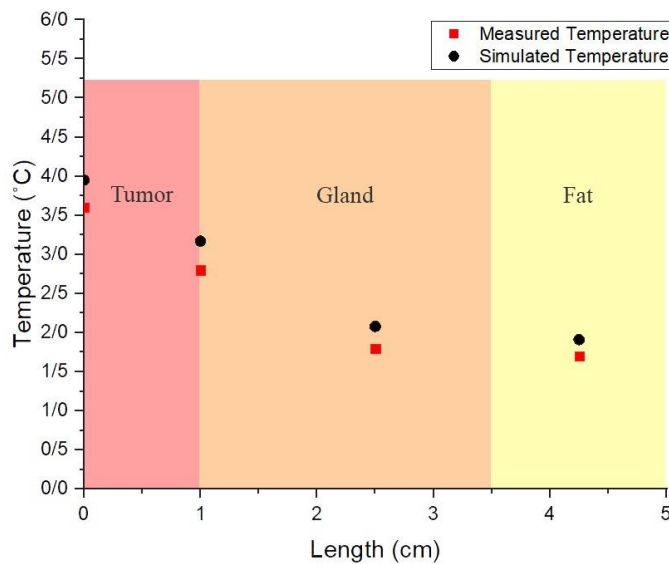


Figure 10. the temperature of phantom in simulation and experimental states; insignificant and negligible difference between two states

Table 4. Increased temperature of different points of phantom in the simulation and experimental studies

Tissues	Experimental temperature	Simulation temperature	Difference temperature	Difference percentage
Tumor	3.6	3.95	+0.35°C	9.7%
T/G Boundary	2.8	3.17	+0.37°C	13.2%
Gland	1.8	2.08	+0.28°C	15.5%
Fat	1.7	1.91	+0.21°C	12.3%

T/G boundary: Tumor and gland boundary

Figure 9 illustrates the isosurface temperature plots in two different views. As shown in figures 7 to 9, the entire region of the tumor reached sufficient heat; nonetheless, the increased temperature of the healthy tissues was about 1.9-2.1°C. To compare the results of the experimental and simulation studies, the achieved temperature of the phantom by both states is depicted in Figure 10. As shown in Table 4, the difference in the temperature of these four points was about 9-15%. This amount of difference protects the experimental conditions and results completely.

Discussion

In this study, the capacitive hyperthermia system was simulated to identify the temperature distribution map and check the operations of the relative devices (i.e., the capacitive hyperthermia and thermometer devices). The RF systems have a significant role in hyperthermia treatments all over the world. However, most of the studies on hyperthermia were investigated in a frequency range which was not widely used in clinical studies [8, 9]. According to the evidence [7], the frequency is inversely proportional to the depth of penetration. In 900 MHz, 4.2 cm depth of body can be reached, and frequencies above this amount cannot be used for breast tumors in clinical treatments. On the other hand, the effects of the capacitive hyperthermia on cancer treatments, especially breast cancer, were not simultaneously investigated in experimental and simulation studies.

In a previous study [18], the effects of RF hyperthermia on breast cancer treatment was investigated in an experimental study. In earlier studies [8, 9], only mimicking the phantom was important. In most studies, the frequency bands were used that were not utilized in clinical treatments, and their RF sources were not employed in clinical devices [4, 8, 9]. Moreover, the consideration of both properties (i.e., the dielectric and thermal properties), which had a role in hyperthermia, was neglected in the simulation and experimental studies [2, 8, 22].

According to the literature [18], the proper mixture with more similarity to the real breast than other mixtures was studied. After measuring important parameters and ensuring that this phantom can well represent real cancerous breast, it was placed in the electromagnetic field that had clinical application in cancer treatment. Because breast tissue contains fat, and the specific heat capacity of fat was lower than other parts, it was very important to have an exact focus point and use power and time that preserve this tissue from

damage. By the measurement of the temperature increasing at different points and calculation of the SAR, a huge achievement in ablation breast cancerous tissues was obtained with this frequency and device. The behavior of this phantom in 13.56 MHz RF hyperthermia device showed an extreme temperature increase in tumor tissue without causing damage to healthy tissues.

Although the experimental results were shown extremely different between the temperature of the healthy and cancerous tissues (1.9-2.1 °C and 3-4 °C, respectively), the condition in the experimental study could have some errors that needed to be discussed. The capacitive device in 13.56 MHz depends on parameters, such as power and time, which have a role in the generated electromagnetic waves between the two electrodes. The function of electrodes and the temperature of water bolus are additional issues. On the other hand, the thermometry system might have some errors. Therefore, the measured temperature could not be individually reliable.

In the previous study, measuring the temperature of all phantom points could not be achieved due to the thermometer device limitations; therefore, calculating the bioheat transfer equation and obtaining the temperature distribution map were extremely difficult and not possible. Moreover, due to the low specific heat capacity of the fat tissue (2280 J/Kg°C), ensuring that this tissue does not damage during the treatment is an important issue. As a result, the investigation of the accuracy of the RF system, precision of the thermometry system, and answer to the bioheat transfer equation were significantly important.

The amount of temperature in the entire phantom is achieved as shown in figures 7-9. However, the temperature of only four points of the phantom was obtained in the previous experimental study. Solving the bioheat transfer equation and obtaining the temperature distribution map showed that all the regions of the healthy tissues were not damaged in this treatment method although the tumor region received adequate heat to cause ablation. Consequently, the simulation results strongly confirmed the experimental results, which protect the treatment method.

Moreover, according to Figure 10, the results of the simulation and experimental study did not have a significant difference (0.21-0.37°C) that describes the satisfactory operation of the RF and thermometry device. Therefore, the simulation results confirmed this fact in the experimental study that tumors can reach adequate temperature; however, the healthy tissues

(especially fat tissues due to their low specific heat capacity) were protected from damage.

According to Table 4, the temperature difference percentage between the simulation and experimental results was about 9-15%. This amount of difference protects the experimental conditions and results completely. As shown in Table 3, the dielectric properties of the tumor tissue are more than healthy tissues. In the hyperthermia method, the higher dielectric properties caused more energy absorption in the electric field of the capacitive system. As a result, the tumor tissue reached a higher temperature (3.6-4°C) than healthy tissues, including the gland and fat tissues (1.8-2.1°C and 1.7-1.9°C).

Conclusion

In this study, the operation of a capacitive hyperthermia system in 13.56 MHz was simultaneously investigated in simulation and experimental study on breast phantom. Since this treatment method has a significant role in cancer therapies, the investigation of the effect of this method on cancer tissue ablation is important. The simulation results strongly supported the experimental results. Although, the healthy tissues (especially fat tissues due to low specific heat capacity) should be protected from extra heating, achieving the temperature distribution map to obtain the temperature of each phantom point is very important. The obtained results showed that the temperature of the whole tumor region increased to approximately 3-4°C.

In addition, the temperature of the completely healthy tissues (i.e., the gland and the fat tissues) did not significantly increase (1.9-2.1°C). Therefore, in the capacitive hyperthermia system, the tumor reaches extreme heat; nevertheless, the healthy tissues can be completely protected from damages. On the other hand, the difference in the temperature of these four points was about 9-15%. This amount of difference completely protects the experimental conditions and results; therefore, the operation of the RF and thermometry device is acceptable.

Acknowledgment

This article has been extracted from the thesis at school of medicine, Tehran University of Medical Science.

References

- González-Díaz C, Uscanga-Carmona MC, Ibarra-Martínez CD, Jiménez-Fernández ME, Lozano Trenado LM, Silva-Escobedo JG, et al. Differentiation BIRADS I vs II by Magnetic Induction Spectroscopy: A Potential Innovative Method to Detect Neoplasies in Breast. *Revista Mexicana de Ingeniería Biomédica*. 2012; 33(2): 65-76
- Stang J, Haynes M, Carson P, Moghaddam M. A preclinical system prototype for focused microwave thermal therapy of the breast. *IEEE Trans Biomed Eng*. 2012; 59(9): 2431-8.
- Yuan Y, Wyatt C, Maccarini P, Stauffer P, Craciunescu O, MacFall J, et al. A heterogeneous human tissue mimicking phantom for RF heating and MRI thermal monitoring verification. *Phys Med Biol*. 2012; 57(7): 2021.
- Miaskowski A, Sawicki B. Magnetic fluid hyperthermia modeling based on phantom measurements and realistic breast model. *IEEE Trans Biomed Eng*. 2013; 60(7): 1806-13.
- Jordan A, Wust P, Scholz R, Tesche B, Fähling H, Mitrovics T, et al. Cellular uptake of magnetic fluid particles and their effects on human adenocarcinoma cells exposed to AC magnetic fields in vitro. *Int. J. Hyperth*. 1996; 12(6): 705-22.
- Nielsen OS, Horsman M, Overgaard J. A future for hyperthermia in cancer treatment?. *Eur. J. Cancer*. 2001; 37(13): 1587-9.
- Joines WT, Zhang Y, Li C, Jirtle RL. The measured electrical properties of normal and malignant human tissues from 50 to 900. *Med Phys*. 1994; 21(4): 547-50.
- Lazebnik M, Madsen EL, Frank GR, Hagness SC. Tissue-mimicking phantom materials for narrowband and ultrawideband microwave applications. *Phys Med Biol*. 2005; 50(18): 4245-58.
- Nguyen PT, Abbosh AM, Crozier S. Thermo-Dielectric Breast Phantom for Experimental Studies of Microwave Hyperthermia. *IEEE Antennas Wirel Propag Lett*. 2016; 15: 476-9.
- Dabbagh A, Abdullah AJJ, Ramasindarum C, Abu Kasim NH. Tissue-Mimicking Gel Phantoms for Thermal Therapy Studies. *Ultrason Imaging*. 2014; 36(4): 291-316.
- Sneed PK, Stauffer PR, McDermott MW, Diederich CJ, Lamborn KR, Prados MD, et al. Survival benefit of hyperthermia in a prospective randomized trial of brachytherapy boost ± hyperthermia for glioblastoma multiforme. *Int J Radiat Oncol*. 1998; 40(2): 287-95.
- Lee TW, Murad Greg JA, Hoh BL, Rahman M. Fighting Fire with Fire: The Revival of Thermotherapy for Gliomas. *Anticancer Res*. 2014; 34(2): 565-74.
- Carpentier A, McNichols RJ, Stafford RJ, Guichard J-P, Reizine D, Delalogue S, et al. Laser thermal therapy: Real-time MRI-guided and computer-controlled procedures for metastatic brain tumors. *Lasers Surg Med*. 2011; 43(10): 943-50.
- Zhou T, Meaney PM, Fanning MW, Geimer ShD, Paulsen KD. Integrated microwave thermal imaging system with mechanically steerable HIFU therapy device. *Spie Bios*. 2009; 7181.
- Mannello F. Understanding breast cancer stem cell heterogeneity: time to move on to a new research paradigm. *BMC Medicine*. 2013; 11(1): 169.
- Velasco-Velázquez M A, Homsí Nora, De La Fuente Marisol, Pestell Richard G. Breast cancer stem cells. *Int. J. Biochem. Cell Biol*. 2012; 44(4): 573-7.
- Al-Hajj M, Wicha MS, Benito-Hernandez A, Morrison SJ, Clarke MF. Prospective identification of tumorigenic breast cancer cells. *Proceedings of the National Academy of Sciences*. 2003; 100(7): 3983-8.
- Kavousi M, Saadatmand E, Alam NR. Physical Parameters Measurement of Breast Equivalent Phantom for Clinical Studies in Radiofrequency

- Hyperthermia. *Frontiers in Biomedical Technologies*. 2019;6(1):28-34.
19. Heydari M, Javidi M, Attar MM, Karimi A, Navidbakhsh M, Haghpanahi M, et al. Magnetic fluid hyperthermia in a cylindrical gel contains water flow. *J Mech Med Biol*. 2015; 15(05): 1550088.
 20. Kok H, Crezee J. A comparison of the heating characteristics of capacitive and radiative superficial hyperthermia. *Int. J. Hyperth*. 2017; 33(4): 378-86.
 21. Pennes H. Analysis of tissue and arterial blood temperatures in the resting human forearm. *J Appl Physiol*. 1998; 85(1): 5-34.
 22. Mukherjee S, Udpa L, Udpa S, Rothwell EJ, Deng Y. Microwave Time-Reversal Mirror for Imaging and Hyperthermia Treatment of Breast Tumors. *Prog Electromagn Res*. 2019; 77: 1-16.